Effect of Reynolds number on aerobreakup of small liquid drops

Taofiq Hasan Mahmood[1], Yue Ling*[1]

[1]Department of Mechanical Engineering, Baylor University, Waco, TX 76798, USA
*Corresponding author email: stanley_ling@baylor.edu

Abstract

Aerobreakup of liquid drops are important to many droplet applications, such as fuel injection. When a liquid drop is subjected to a gas stream of high velocity, the drop can deform and break into small droplets. The drop aerobreakup is controlled by multiple dimensionless parameters. The Weber number (We) has been commonly used to characterize the different breakup regimes. While the effects of Weber and Ohnesorge numbers on the aerobreakup of a drop in unbounded domain have been extensively studied, the effect of the Reynolds number (Re) based on gas properties are less understood and will be investigated by 2D axis-symmetric and 3D detailed numerical simulations in the present paper. Attention will be focused on the moderate We regime, where the drop mostly breaks in the bag mode. In many previous studies for millimeter drops, Re is too large to be relevant. However, for applications where drops are small and the relative velocity is high, Re can be quite small when the drop breaks. Parametric simulations of Re and We are performed to systematically investigate the effect of Re on the drop aerobreakup dynamics. The simulations are performed using the Basilisk solver, where the mass-momentum consistent VOF method is used to capture the interfacial dynamics on an adaptive mesh. The reduced Re is found to induce significant changes in the drop acceleration, deformation, bag morphology, and the bag breakup dynamics, which in turn lead to significant variation in the size and spatial distributions of the children droplets formed.

Keywords

Aerobreakup, Secondary atomization, Direct numerical simulation.

Introduction

When a drop is subjected to a gas flow, the drop-gas interaction causes drop deformation. If the stabilizing surface tension and viscous forces are not sufficient to overcome the inertia force, the drop will break. This drop aerobreakup process is important to many applications, such as fuel injection and atomization in combustion engines and raindrop damage on supersonic vehicles.

The study of drop aerobreakup is generally formulated as a liquid drop of density ρ_l, viscosity μ_l, and diameter D_0 subjected to a uniform gas stream with density ρ_g, viscosity μ_g, velocity U_0, and surface tension σ, in an unbounded domain. Therefore, the problem can be fully characterized by four independent dimensionless parameters: the Weber number $We = \rho_g U_0^2 D_0/\sigma$, the Reynolds number $Re = \rho_g U_0 D_0/\mu_g$, and the gas-to-liquid density and viscosity ratios $r = \rho_g/\rho_l$ and $m = \mu_g/\mu_l$. Dimensionless parameters other than the four mentioned above have also been used [1, 2]. In particular, when the drop liquid is highly viscous, the viscosity ratio m can be replaced by the Ohnesorge number $Oh = \mu_l/\sqrt{\rho_l D_0 \sigma}$. For low Oh, the surface tension dominates, so that We characterizes different aerobreakup regimes.

The previous studies on drop aerobreakup are mainly based on experiments [3, 4], using shock tubes [5, 6, 7, 8] and continuous jets in wind tunnels [9, 1]. The experimental results have lead to a regime classification for $Oh \ll 1$: *vibrational* ($We \lesssim 11$), *bag* ($11 \lesssim We \lesssim 35$), *multimode* ($35 \lesssim We \lesssim 80$), and *sheet-thinning* ($We \gtrsim 80$), based on drop morphology. The aerobreakup has also been classified as Rayleigh-Taylor piercing (RTP) and shear-induced entrainment (SIE) regimes, based on the destabilizing mechanisms [8, 4]. For high-viscosity

liquids or high-pressure liquids approaching the thermodynamic critical point, the threshold values for We for different regimes generally increases with Oh [10, 11]. Recent numerical studies showed that the density ratio r can also influence aerobreakup when $r > 0.01$ [2, 12].
While the former studies of drop aerobreakup are mainly focused on millimeter drops, submillimeter drops can also break when they are subjected to high-speed gas flows. For millimeter drops, the typical values of Re is too large to be relevant, nevertheless, when the drop size is reduced, the Re will decrease and the effect of Re can be significant. If the fluid properties are fixed, we can keep We unchanged by varying U_0 and D_0 simultaneously, resulting in scaling relation $Re \sim D_0^{1/2}$. For example, for $We = 11$, the corresponding Reynolds numbers for $D_0 = 3$ mm and 30 μm are $Re = 2970$ and 297, respectively. For such a large decrease of Re, the gas flow around the drop will vary significantly [13], and will in turn influence the acceleration, deformation, and breakup of the drop. Few studies in the literature address the effect of Re on the aerobreakup of drops. Aalburg *et al.* [14] claimed that Re is not important if $Re > 100$. However, their conclusion was made based on simulation results for non-broken drops for one density ratio ($r = 0.031$). More recent simulations by Jain *et al.* [12] showed that the drop morphology changes significantly with Re even for $Re > 1000$. It is obvious that a comprehensive understanding of the effect of Re along with other important parameters remains to be established. For drops as small as microns or tens of microns, visualizing and measuring drop breakup in experiments is very difficult, therefore, high-fidelity numerical simulation is an essential alternative to investigate the problem.
The goal of the present study is to characterizing the effect of Reynolds number on drop aerobreakup. The free-stream velocity and the drop diameters are varied to cover wide ranges of We and Re. Due to the interest of small submillimeter drops, We is moderate, so the drop breakup, if occurs, will mainly be located in the bag breakup regime or at most the lower end of sheet-thinning regime. Both 2D axisymmetric and 3D simulations will be performed. While the former are less expensive, so a parametric study will be performed to characterize the the effect of Re on the breakup criterion, the latter will be used to illustrate the 3D breakup features for representative cases.

Simulation methods

Governing equations

The two-phase interfacial flows are governed by the incompressible Naviers-Stokes equations with surface tension,

$$\rho\left(\frac{\partial u_i}{\partial t} + u_i\frac{\partial u_j}{\partial x_j}\right) = -\frac{\partial p}{\partial x_i} + \frac{\partial}{\partial x_j}\left[\mu\left(\frac{\partial u_i}{\partial x_j} + \frac{\partial u_j}{\partial x_i}\right)\right] + \sigma\kappa\delta_s n_i\,, \tag{1}$$

$$\frac{\partial u_i}{\partial x_i} = 0\,. \tag{2}$$

where ρ, u_i, p, μ represent density, velocity, pressure and viscosity, respectively. The Dirac distribution function δ_s is localized on the interface. The surface tension is denoted by σ, while κ and n_i represent the curvature and normal vector of the interface.
The gas and liquid phases are distinguished by the liquid volume fraction c, the evolution of which follows the advection equation:

$$\frac{\partial c}{\partial t} + u_i\frac{\partial c}{\partial x_i} = 0\,. \tag{3}$$

Numerical methods

The governing equations (Eqs. (1), (2), and (3)) are solved using the open-source, multiphase flow solver *Basilisk* [15]. The *Basilisk* solver uses a finite-volume approach based on a projection method. An adaptive quadtree spatial discretization is used, which allows for adaptive mesh refinement (AMR) in user-defined regions. The advection equation (Eq. (3)) is solved via

Table 1. Physical parameters.

	ρ_l (kg/m^3)	ρ_g (kg/m^3)	μ_l (Pa s)	μ_g (Pa s)	σ (N/m)	D_0 (m)	U_0 (m/s)
Case 1	1110	1.2	1.61×10^{-2}	1.8×10^{-5}	0.0483	2.7×10^{-3}	15 & 18
Case 2	659	3.5	3×10^{-3}	2.86×10^{-5}	0.0127	$1.8 \times 10^{-6} - 2.3 \times 10^{-2}$	$1 - 266$

Table 2. Key dimensionless parameters.

	r ρ_g/ρ_l	m μ_g/μ_l	Re $\rho_g U_0 D_0/\mu_g$	We $\rho_g U_0^2 D_0/\sigma$
Case 1	1.0×10^{-3}	1.1×10^{-3}	2700 & 3240	15.1 & 21.7
Case 2	5.3×10^{-3}	3.48×10^{-2}	$50 - 3200$	$8 - 120$

the piecewise-linear geometrical Volume-of-fluid (VOF) method [16, 17]. The balanced-force method is used to discretize the surface tension term [17]. The height-function (HF) method is used to calculate the local interface curvature [17]. The *Basilisk* solver utilizes a staggered-in-time discretization of the volume fraction/density and pressure, leading to a formally second-order-accurate time discretization [17]. Numerous validation studies for the numerical methods, as well as examples of a wide variety of interfacial multiphase flows, can be found on the *Basilisk* website and in previous studies.

Physical parameters and simulation cases

Two different combinations of gas and fluid properties are considered, see Table 1. While the case 1 are for Ethylene-glycol drop in air, the case 2 is for isooctane drop in high-pressure nitrogen, following the ECN spray G condition. The dimensionless parameters are summarized in Table 2. Using D_0, U_0 as the scaling variables, the dimensionless variables, indicated by a superscript *, are defined, *e.g.*, $t^* = tU_0/D_0$, $u^* = u/U_0$ and $x^* = x/D_0$.

For case 1, two different free-stream velocities are considered, $U_0 = 15$ and 18 m/s. The parameters for the case 1 with $U_0 = 15$ m/s is identical to one of the experimental case of Opfer *et al.* [1], which are used for validation. For the case 2, the density and viscosity ratios are kept as constant, and the free-stream velocity and the drop diameters are varied to cover wide ranges of We and Re. Eight different Weber numbers, *i.e.*, $We = 8,\ 9,\ 10,\ 11,\ 13,\ 15,\ 25,\ 50,\ 120$, and seven different Reynolds numbers, *i.e.*, $Re = 50,\ 100,\ 200,\ 400,\ 800,\ 1600,\ 3200$, are considered. The cases with very large We and very small Re, for which the free-stream will become supersonic, are excluded. Therefore, about 53 2D-axisymmetric runs are made for case 2. Since the 3D simulations are computationally expensive, three different Re are considered, namely $Re = 100,\ 400,\ 1600$ when We is fixed at 25. The value of Oh varies from 0.0007 to 0.07, which is small in general, so that the effect of liquid viscosity is secondary according to the previous studies [11].

Simulation setup

The computational domains for the 2D-axisymmetric and 3D simulations are schematically shown in figure 1. For both setups, uniform inflow boundary condition (BC) is applied on the left surface of the domain, while the BC on the right boundary is pressure outflow. All lateral boundaries are considered as slip walls, except that for the bottom of the 2D setup is axis-symmetric. The 2D domain is a rectangular box with dimensions l_x and l_y, while l_x is fixed at $17.5D_0$, l_y is varied to investigate the effect of confinement. The computational domain for the 3D setup is a cube with edge length $l = 16D_0$. For both setups, the drop is initially placed $x_0 = 3D_0$ away for the inlet. For the 3D simulation, the initial location of the drop is at the center of y-z plane.

The adaptive quadtree/octree mesh is used to discretize the domains. The minimum cell size Δ is controlled by the maximum refinement level L. For the 2D setup, $L = 12$, which corresponds to 512 cells across the initial drop diameter D_0. While for 3D simulations, $L = 11$. The 2D simulations are run on the campus cluster *Kodiak* using 4 cores, and each run takes about 10 hours. The 3D simulations are run on the TACC-Stampede2 machine using 768 cores and each run takes about 10 days.

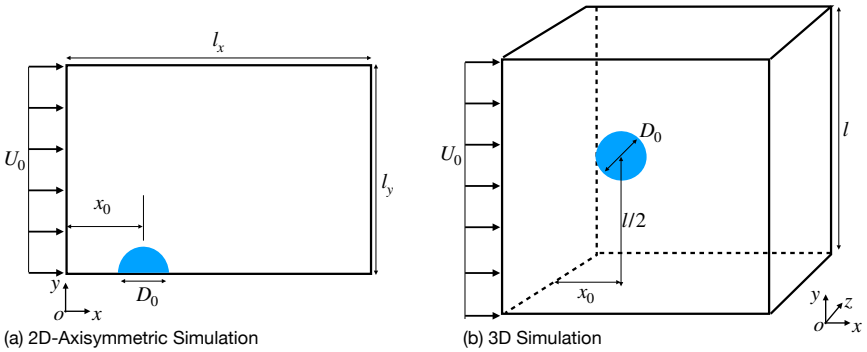

Figure 1. Schematics of the computational domains for (a) 2D-axisymmetric and (b) 3D simualtions.

Results and discussion

General behavior

The general behavior of the aerobreakup of a liquid drop is shown in Fig. 2. The results are for the millimeter Ethylene-glycol drop ($D_0 = 2.7$ mm) of case 1 with $We = 21.7$ and $Re = 3240$. The drop is initially stationary, and at time zero is exposed to a free stream from left to right. The morphological evolution demonstrated in Fig. 2(a) is consistent with previous experimental and numerical studies [4, 1, 12]. The initially spherical drop (I) is flattened to a disk (II). Due to the increase of frontal cross section area, the drop acceleration increases, see Fig. 2(d) for the drop velocity u_c^*. The accelerating upstream surface of the disk is unstable due to the Rayleigh-Taylor instability. As a result, the center region of the disk becomes thinner and bends toward the streamwise direction, turning the disk to a bowl shape (III). Up to this stage, the drop is still approximately axisymmetric and the lateral diameter of the drop D^* increases approximately linearly in time, see Fig. 2(b). Then the bowl is quickly inflated to form a forward facing bag (IV), the symmetry breaks down, and the length of the drop rises in time rapidly, see Fig. 2(c). For this specific case, two bags are observed and the bottom one breaks first (V), followed by the second one. Multiple holes are formed at the same time and the merging of the holes cause the bags to break violently. The unbroken sheet at the center of the bag and the unbroken rim will continue to break due to the interaction with the gas stream, forming drops that are significantly larger than those from the holes-induced breakup of the bags.

The results for 2D axisymmetric simulations with the same parameters using a coarser and finer meshes (L=10 and 12) are shown for comparison and are observed to agree well with the 3D results in general. Very good agreement is observed up to about $t^* \approx 40$, when the bag changes from the bowl to bag shapes. This indicates the 2D axisymmetric simulations are capable to capture the drop deformation until the bag is inflated, which is thus useful to identify whether the drop breakup regime. When the bag grows and break, the discrepancy between the two setups will increase, indicating the 3D simulations are required to capture the bag breakup dynamics and the statistics of the outcome children droplets.

Effect of confinement

The results for the case 1 with $We = 15$ and $Re = 2700$ for different domain height l_y are shown in Fig. 3 to illustrate the effect of boundary confinement on the drop aerobreakup. The case

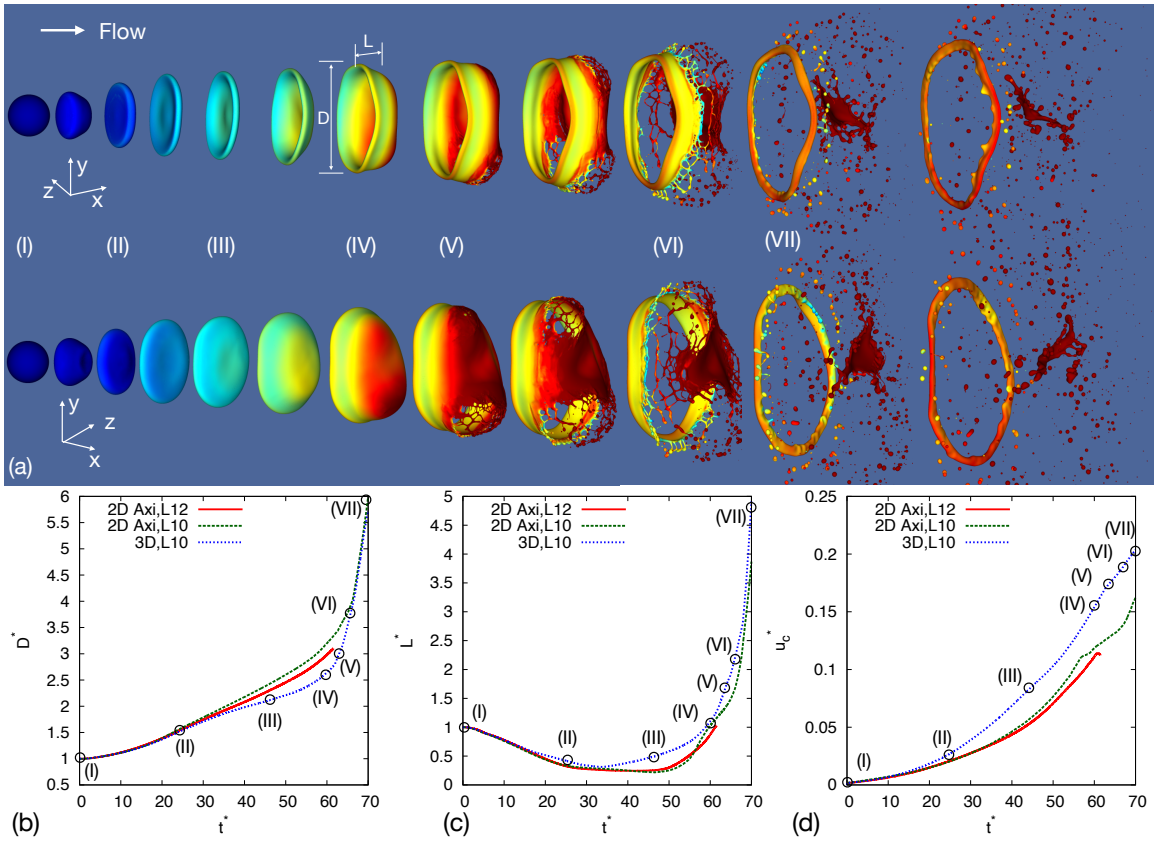

Figure 2. Temporal evolution of (a) the drop surfaces, (b) lateral diameter D^*, (c) longitudinal length L^*, and (d) central velocity u_c^* for the aerobreakup of a liquid droplet corresponding to case 1 with $r = 10^{-3}$, $m = 1.1 \times 10^{-3}$, We $= 21.7$ and Re $= 3240$. In (a), the drop surface is colored by the velocity magnitude.

simulated here is identical to the experiment of Opfer [1], which is later simulated by Marcotte and Zaleski [2] using the solver *Gerris*. It can be observed that the effect of l_y is almost invisible up to about $t^* = 40$, when the bag has not yet been formed. As D^* becomes large, the results for different l_y start to deviate from each other. It is interesting to notice that the results with a narrow domain $l_y/R_0 = 5$, where $R_0 = D_0/2$ is the initial drop radius, agree the best with the experiment. This domain height is also what Marcotte and Zaleski [2] used in the simulation. For $l_y/R_0 > 7.5$, namely the distance of the lateral wall to the drop center is larger than about $7.5R_0$, the effect of confinement on the drop deformation and drop velocity evolution becomes small. The difference between the results for $l_y/R_0 = 12.5$ and $l_y/R_0 = 17.5$ are almost invisible. Therefore, l_y and l are set to 16 for the rest 2D axis-symmetric and 3D simulations to avoid the confinement effect.

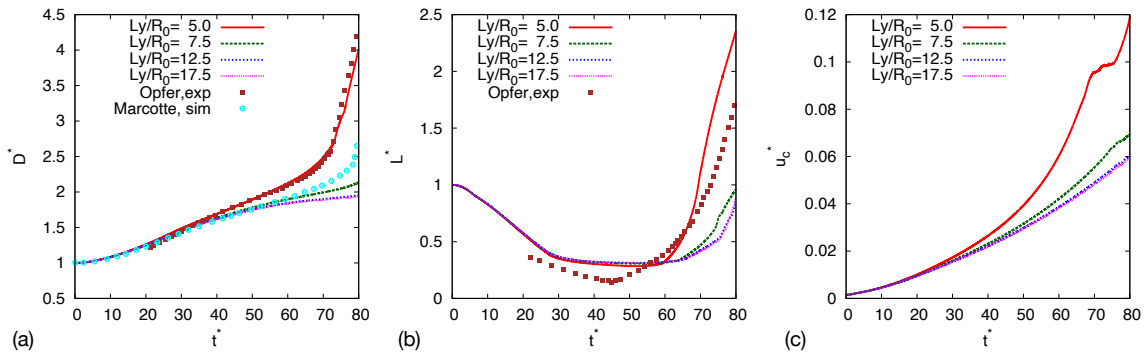

Figure 3. Temporal evolution of (a) lateral diameter D^*, (b) longitudinal length L^*, and (c) central velocity u_c^* for case 1 with $r = 10^{-3}$, $m = 1.1 \times 10^{-3}$, We $= 15.1$ and Re $= 2700$ for different domain heights l_y.

Effect of Reynolds number on drop deformation and breakup

The temporal evolutions for D^*, L^*, and u_c^* for different Re and We and the case 2 are shown in Fig. 4. The three We shown here correspond to the bag, multi-mode, and shear breakup modes when Re is large, *e.g.*, $Re > 1600$. If the drop breaks, the time period when breakup occur is marked by symbols in the figures. In the present simulations, the pinching of the liquid sheet occurs when the sheet thickness is less than the minimum cell size. Therefore, the breakup time will vary slightly when the mesh resolution changes. Nevertheless, since the liquid sheet thickness decreases very rapidly near the breakup time, results from grid-refinement study indicate that the variation of the precise breakup time is very small when the minimum cell size is reduced.

When Re decreases, the results for D^* and L^* are initially similar, but deviations start to show up at later time. The smaller Re, the earlier the deviation starts. Consistent for all three We, D^* is reduced when Re decreases. Consistently, the drop is flattened to a thicker disk, see the increase of L^* in the plateau for $10 \lesssim t^* \lesssim 20$ for $We = 13$. These changes in drop deformation is clearly tied to the change of drop acceleration as shown in Fig. 4(c). The decrease in Re results in a higher acceleration of the drop from the beginning. It is observed that the changes in u_c is more profound when We decreases, which explains why the effect of Re on drop deformation is the most significant for $We = 13$. For $We = 13$, the breakup time increases with decreasing Re and for $Re \leq 200$, no breakup is observed. For $We = 25,\ 120$, the variation of the breakup time with Re is non-monotonic.

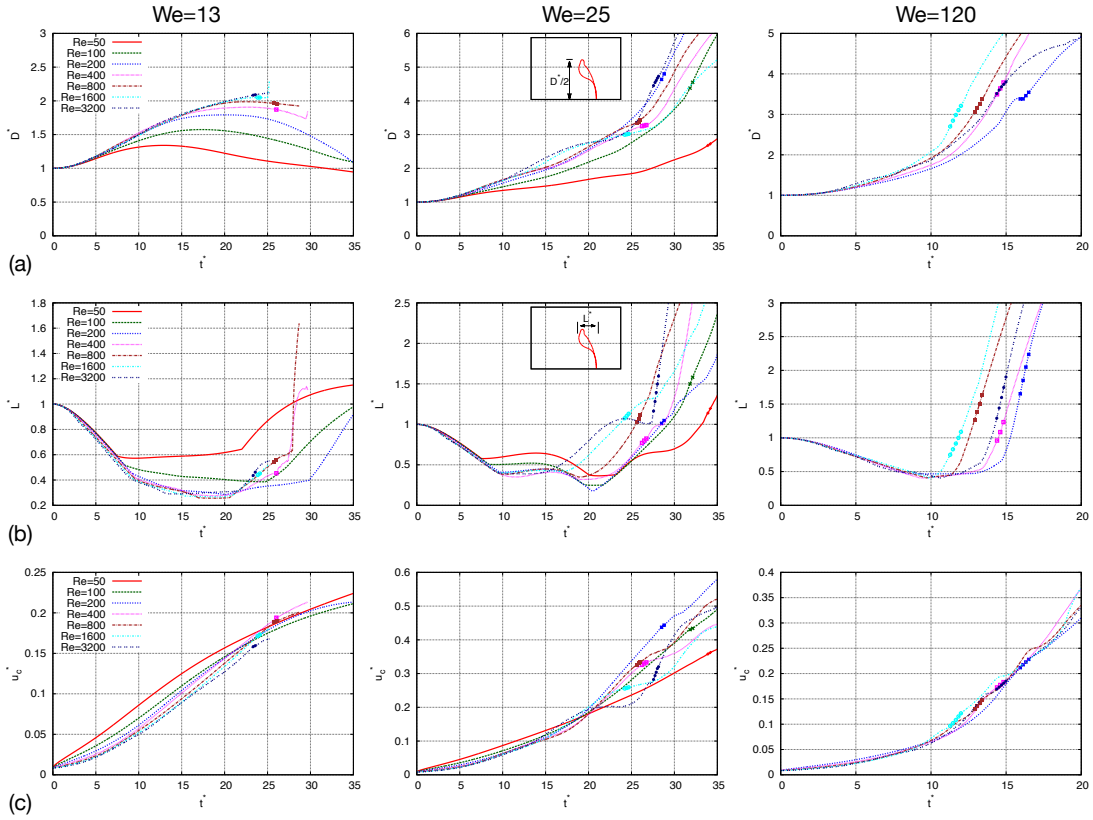

Figure 4. Temporal evolutions of (a) lateral diameter D^*, (b) longitudinal length L^*, and (c) central velocity u_c^* for case 2 with $r = 5.3 \times 10^{-3}$, $m = 3.48 \times 10^{-3}$ and different We and Re. The breakup time is marked by symbols.

Representative snapshots of the drop surfaces for different Re and We and the case 2 are shown in Fig. 5. The colors for each We correspond to the same times. The effect of Re on the deformation and breakup of the drop for different We can be identified. The effect is again most profound for $We = 13$, for which the drop changes from a forward bag breakup to no breakup, when Re reduces from 3200 to 200. This indicates that the critical We_{cr} that determines if the

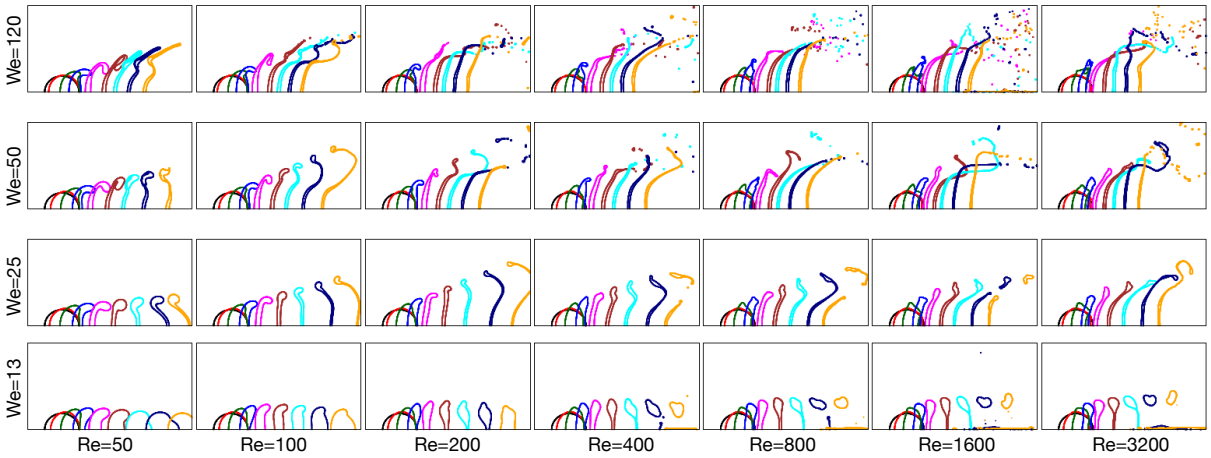

Figure 5. Deformation and breakup of the drops for case 2 and different We and Re.

drop breaks will increases when Re decreases. It is also interesting to notice that for $We = 25$, the bag morphology changes from a backward bag, to backward-to-forward-transient bag, to a forward bag when when Re decreases. This change in bag morphology will influence the breakup dynamics and the size and velocity distributions of the drops formed. For $We = 120$, the drops all deform to backward bags with small drops dripped from the edge, which is typical for the shear breakup. The effect of Re is only reflected in the intensity of breakup.

Effect of Reynolds number on 3D breakup features

The morphological evolutions for $Re = 100$, 400, and 1600 for the case 2 and $We = 25$ are shown in Fig. 6. The variation in the bag morphology when Re varies can be clearly seen. For this moderate We, the drop breakup is in the bag mode. For the small $Re = 100$, a forward bag is formed. In contrast, for large $Re = 1600$, a backward bag is formed. When Re is intermediate, *i.e.*, $Re = 400$, a combination of the two modes is observed, leading to the Sombrero hat drop shape. The change in the bag morphology clearly influences the statistics of the children drops formed. For $Re = 1600$, the lateral spread of the drop is narrower, the formed droplets are thus distributed much closer to the axis. Furthermore, the major rim of the bag is also thicker, the breakup of which will lead to larger droplets.

Conclusions

The effect of the gas Reynolds number Re on drop aerobreakup has been investigated by 2D axis-symmetric and 3D interface-revolved simulations. The effect of Re is found to be important to the deformation and breakup dynamics, in particularly for low Weber numbers We. The critical We_{cr} for the onset of breakup increases with decreasing Re. In the bag breakup regime, when Re increases, the bag morphology can vary from backward bag, Sombrero hat, to forward bag. The change of bag morphology also influences the size and spatial distributions of the droplets formed. A quantitative analysis of the effect of Re on the drop statistics will be performed in the future and the long-term goal is to establish sub-grid models for drop breakup using the simulation data, which can be used in Lagrangian point-particle simulations.

Acknowledgements

This research was supported by the National Science Foundation (#1853193). The authors also acknowledge TACC for providing the computational resources for the present simulations.

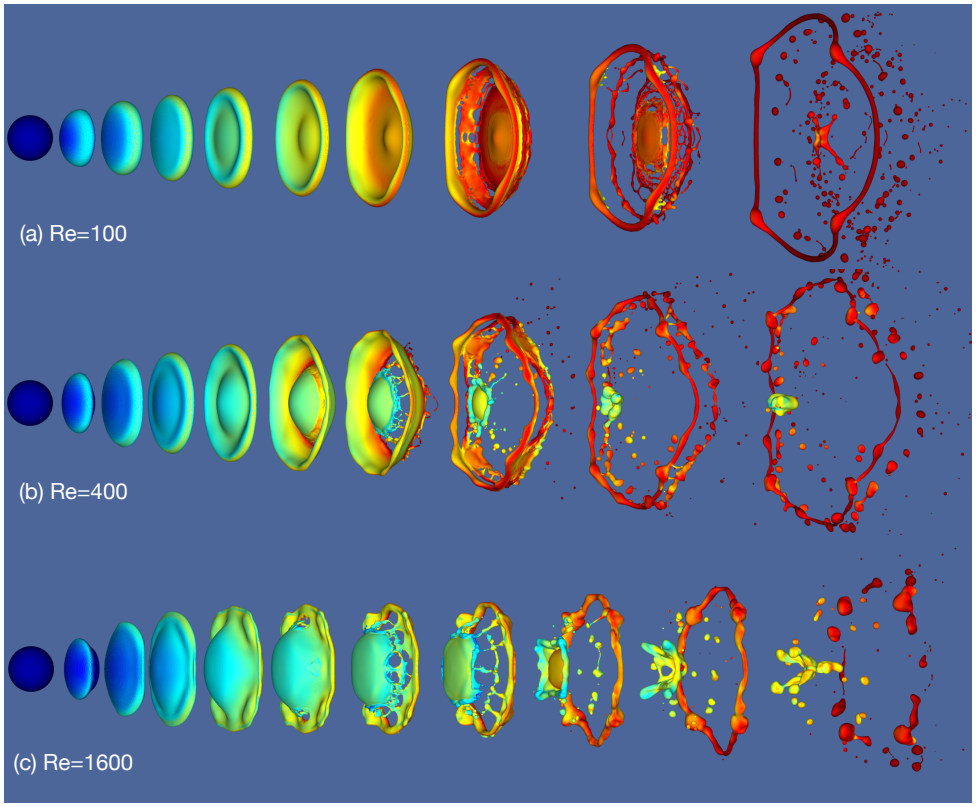

Figure 6. 3D simulation results of drop deformation and breakup for the case 2 and We $= 25$, for (a) Re $= 100$, Re $= 400$, and Re $= 1600$.

References

[1] Opfer, L., Roisman, I. V., Venzmer, J., Klostermann, M. and Tropea, C. "Droplet-air collision dynamics: Evolution of the film thickness." *Phys. Rev. E* Vol. 89 (2014): p. 013023.

[2] Marcotte, F. and Zaleski, S. "Density contrast matters for drop fragmentation thresholds at low Ohnesorge number." *Phys. Rev. Fluids* Vol. 4 (2019): p. 103604.

[3] Guildenbecher, D. R., López-Rivera, C. and Sojka, P. E. "Secondary atomization." *Exp. Fluids* Vol. 46 (2009): p. 371.

[4] Theofanous, T. G. "Aerobreakup of Newtonian and viscoelastic liquids." *Annu. Rev. Fluid Mech.* Vol. 43 (2011): pp. 661–690.

[5] Hinze, J. O. "Fundamentals of the hydrodynamic mechanism of splitting in dispersion processes." *AIChE J.* Vol. 1 (1955): pp. 289–295.

[6] Hsiang, L.-P. and Faeth, G. M. "Drop deformation and breakup due to shock wave and steady disturbances." *Int. J. Multiphase Flow* Vol. 21 (1995): pp. 545–560.

[7] Joseph, D. D., Belanger, J. and Beavers, G. S. "Breakup of a liquid drop suddenly exposed to a high-speed airstream." *Int. J. Multiphase Flow* Vol. 25 (1999): pp. 1263–1303.

[8] Theofanous, T. G., Li, G. J. and Dinh, T.-N. "Aerobreakup in rarefied supersonic gas flows." *J. Fluid Eng.-T. ASME* Vol. 126 (2004): pp. 516–527.

[9] Liu, A. B. and Reitz, R. D. "Mechanisms of air-assisted liquid atomization." *Atomization Spray* Vol. 3 (1993): pp. 55–75.

[10] Faeth, G. M., Hsiang, L.-P. and Wu, P.-K. "Structure and breakup properties of sprays." *Int. J. Multiphase Flow* Vol. 21 (1995): pp. 99–127.

[11] Theofanous, T. G., Mitkin, V. V., Ng, C. L., Chang, C. H., Deng, X. and Sushchikh, S. "The physics of aerobreakup. II. Viscous liquids." *Phys. Fluids* Vol. 24 (2012): p. 022104.

[12] Jain, S. S., Tyagi, N., Prakash, R. S., Ravikrishna, R. V. and Tomar, G. "Secondary breakup of drops at moderate Weber numbers: Effect of Density ratio and Reynolds number." *Int. J. Multiphase Flow* Vol. 117 (2019): pp. 25–41.

[13] Feng, J. Q. "A deformable liquid drop falling through a quiescent gas at terminal velocity." *J. Fluid Mech.* Vol. 658 (2010): pp. 438–462.
[14] Aalburg, C., Van Leer, B. and Faeth, G. M. "Deformation and drag properties of round drops subjected to shock-wave disturbances." *AIAA J.* Vol. 41 (2003): pp. 2371–2378.
[15] Popinet, S. "The Basilisk Code." Available from http://basilisk.fr/.
[16] Scardovelli, R. and Zaleski, S. "Direct numerical simulation of free-surface and interfacial flow." *Annu. Rev. Fluid Mech.* Vol. 31 (1999): pp. 567–603.
[17] Popinet, S. "An accurate adaptive solver for surface-tension-driven interfacial flows." *J. Comput. Phys.* Vol. 228 No. 16 (2009): pp. 5838–5866.